Afar triple junction fed by single, asymmetric mantle upwelling

Emma J. Watts[1*], Rhiannon Rees[1], Thomas M. Gernon[1], Philip Jonathan[2,3], Derek Keir[1,4], Rex N. Taylor[1], Melanie Siegburg[5], Emma L. Chambers[6], Carolina Pagli[7], Matthew J. Cooper[1], Agnes Michalik[1], J. Andrew Milton[1], Thea K. Hincks[1].

[1]School of Ocean and Earth Science, University of Southampton, National Oceanography Centre, European Way, Southampton, SO14 3ZH, UK

[2] Department of Mathematics and Statistics, Lancaster University, Lancaster, UK

[3]Shell Research Limited, London, UK

[4] Dipartimento di Scienze della Terra, Università degli Studi di Firenze, Firenze 50121, Italy

[5] Landesamt für Geologie und Bergwesen Sachsen-Anhalt, Halle (Saale), Germany

[6] School of Cosmic Physics, Dublin Institute for Advanced Studies, Dublin, Ireland

[7] Dipartimento di Scienze della Terra, Università di Pisa, Pisa 56126, Italy

*Corresponding Author Email: e.watts@soton.ac.uk

Mantle upwellings drive large-scale surface volcanism and facilitate continental breakup and the formation of ocean basins [1-3]. However, the spatial characteristics of these upwellings directly below the Earth's crust remain enigmatic. The classic Afar triple junction in East Africa comprises three rifts at varying stages of evolution, thus allowing us to examine their spatial expression and factors that control them. Afar is widely considered to be underlain by a deep-sourced and broad mantle hotspot or plume [4, 5], although the existence of such a plume has been hotly contested [6]. Here, we present extensive new geochemical and isotopic data spanning the triple junction to show that the mantle beneath Afar consists of a single, asymmetric heterogeneous upwelling. Using statistical modelling approaches to integrate our new geochemical data with existing

geophysical datasets, we identify an upwelling exerting a fundamental control on the composition and abundance of melt in all three rifts. Within each rift arm, we identify variations in mantle compositions on characteristic length scales of about 50 to 200 km. These length scales are longer in the more advanced and faster-extending rift sectors, suggesting more rapid channelised flow. Our findings elucidate the spatially heterogeneous characteristics of mantle upwellings [7, 8, 9] and demonstrate their susceptibility to the dynamics of overriding plates.

Introduction

Mantle plumes or hotspots, that is, upwellings of the mantle that originate between 1,000 and 2,800 km [10], are anomalously hot zones of the mantle and/or of an enriched composition which reduces the solidus temperature favouring partial melting [10]. The role of mantle plumes (hereafter, upwellings) in driving volcanism during continental breakup has long been debated, but with only a small fraction of Earth's upwellings situated under continents [11] and a limited number of upwellings associated with active continental rifting [12], our understanding of rift-upwelling interactions remain incomplete. In the 'classic' magma assisted continental rift, the Afar triple junction—where the Arabian, Nubian, and Somalian tectonic plates intersect—all three rifts are currently active [13], making it an ideal location to study the interactions between mantle upwelling and continental rifting. Here, the driver of melt production is debated with some models suggesting decompression melting with minimal upwelling involvement [6], while others propose the upwelling of hot, deep mantle [14], or even multiple upwellings [15, 16]. Whilst several discrete segments of the rift have been studied in terms of magma petrogenesis (e.g., [14, 17]), a paucity of high-precision geochemical data has hampered our ability to comprehensively evaluate the spatial characteristics of upwelling across the broader region and thereby rigorously test these models.

Probing the presence of a mantle upwelling

To overcome this limitation, we begin our study by implementing a comprehensive sampling strategy, targeting young volcanoes spanning all three rift systems (Fig. 1). Specifically, we target rocks that are Quaternary in age (i.e., less than 2.58 million years (Myr) old), and from volcanoes that have been active during the Holocene period, which began 11.7 thousand years ago (ka) [18]. By targeting younger rocks, we aim to make a direct comparison with geophysical data across the region, enabling an integrated exploration of mantle petrogenesis and dynamics.

Our new compilation includes over 150 rock samples, more than doubling the number of high-quality analyses in the area, with many of these from previously unstudied volcanoes. These samples were carefully selected from a repository covering the broader Afar region (see Methods for details), supplemented by additional samples collected during fieldwork in the Main Ethiopian Rift (MER). To examine spatial trends in the geochemistry of surface volcanism, all samples were analysed for major and trace elements alongside radiogenic isotopes (Sr, Nd, Pb; see Methods). We also integrate high-quality data from the open-source GEOROC data repository (https://georoc.eu/ [21]) for rocks, including the classic catalogue from [16] (i.e., the Gulf of Aden), where a complete set of analyses was available within the area of interest. Additionally, we leverage recent spatial maps of key geophysical variables, such as the depth of the Mohorovičić Discontinuity (see Methods for further details) and shear wave velocities at regularly spaced depths (i.e., 40, 60, 80, 100, and 120 km [22]). These variables provide well-established proxies for the boundary between the crust and mantle, as well as for the presence and abundance of melt within the lithosphere and asthenosphere [22]. Collectively, this information allows us to infer details about the depth, extent, and compositional characteristics of melts distributed spatially across all three rifts.

Mantle upwellings, commonly associated with reduced seismic velocities (Vs, Vp) [24, 25], are widely accepted to tap a deep-mantle component called C (common [23]) and/or FOZO (focus zone [26]). Such components typically exhibit an isotopically distinct composition (that is, generally low $^{87}Sr/^{86}Sr$, high $^{143}Nd/^{144}Nd$, and high $^{206}Pb/^{204}Pb$ [26]) and elevated trace element ratios ($\Delta Nb > 0$, see Eq. A1 [27]; $Ce/Pb > 30$). We find that all samples within our study region, specifically, within 500 km of the Afar triple junction, exhibit strong C/FOZO signatures (Figs. 1 and Extended Data Fig. 1), supporting a first-order deep upwelling control on the composition and abundance of melt [16, 25, 26]. When we apply a spline interpolation to the data (Methods), we detect prominent isotopic and geochemical variations across the broader region (Fig. 1). This includes distinctly elevated La/Sm, Ce/Pb, and $^{206}Pb/^{204}Pb$, and decreased $^{87}Sr/^{86}Sr$ and shear wave speeds in northern Afar, central Afar (near the triple junction), and sporadically along the MER and Gulf of Aden Rift (Figs. 1 and Extended Data Fig. 1). These spatial trends implicate an underlying complexity to magmatism and mantle upwelling, which has previously been inferred using geophysical approaches (e.g., [22, 29, 30, 31]).

These data and observations enable us to test multiple models of mantle upwelling dynamics. The first model we consider is a simple, homogeneous mantle upwelling impinging at the triple junction (e.g., [16]), which is expected to produce a systematic shift in variables traditionally taken to indicate deep upwelling radially with distance (Fig. 2). Extending this model, we then allow the upwelling to be spatially and temporally heterogeneous, as reported in the Hawaiian [32] and Canary Island [9] volcanoes. This mechanism yields a similar pattern to the first model centred at the triple junction, but accommodate compositional fluctuations over the radial distance corresponding to the arrival of chemically distinct pulses (Fig. 2).

We additionally test whether the spatial variations observed (Figs. 1 and Extended Data Fig. 1) are best explained through the presence of numerous small-scale upwellings, which have been proposed based on geophysics and numerical models (e.g. [30]). Using the data summarised in hex-maps (Figs. 1 and Extended Data Fig. 1), we test this model using three upwellings: one centred on the triple junction, one on the Red Sea Rift north of the Afar region, and one in the southern MER, with the positions of these loci informed by previous observations (see Methods). The strong mantle signatures observed across the wider area (Figs. 1 and Extended Data Fig. 1b) suggest that crustal assimilation has played a relatively minor role in recent magmatism. This inference is consistent with geochemical and isotope evidence, which indicate that crustal assimilation was much more significant during earlier stages of rifting, at approximately 30 Ma, when the continental crust was thicker and magmatic fluxes were higher [33]. In contrast, the current crust is heavily thinned and has been intruded by mafic melts along the length of the rift axes. Seismic analysis indicates that recent magmatic activity beneath the rift axis in Afar is transient [34] and, in turn, that magmas are unlikely to reside in crustal reservoirs for long enough to extensively assimilate crustal lithologies.

To interrogate this further, we explore the correlation between key geochemical and geophysical indicators (Fig. 3b) and the depth to the Moho (boundary between crust and mantle used to indicate crustal thickness), as crustal thickness is widely thought to influence the degree of assimilation [33] (Methods). We found that most indicators, including Pb isotopes—a reliable indicator for crustal assimilation [35]—exhibit only a weak, but significant, correlation with the Moho depth (Fig. 3b). On the other hand, Ce/Pb exhibits a strong negative correlation (i.e., Pearson correlation coefficient of -0.7), indicating that where the crust is thin, the Ce/Pb values are high, and vice versa. This trend can be attributed to minimal crustal assimilation across most of the region, but increasing as the crust thickens

within the MER. Nevertheless, we test this further by excluding cases where Ce/Pb values fall below 20 and which could feasibly be associated with crustal assimilation [35].

Afar Mantle Upwelling's Spatial Characteristics

To test between a singular upwelling (hereafter, model 'C1C') and small-scale upwellings (model 'C3C'), we identify 13 key geochemical and geophysical variables (Extended Data Table 2) and calculate the distance, using the spherical cosine law (see Methods), between the purported upwelling centre [5, 16, 36] and each observation site (Methods). We then apply two-deep cross validation to find the optimum linear fit (that is, representing a homogeneous upwelling) and penalised B-spline fit (that is, representing a heterogeneous upwelling) to each of the variables over a radial distance of 500 km—the radial limit of data points considered within this study (Fig. 3c and Extended Data Fig. 2). The predictive performance of each fit is then assessed by calculating the mean standardised root-mean squared error of prediction (RMSEP; Fig. 3a), where a value of 1 indicates a lack of predictive capability, and 0 a perfect predictive ability. For both models (C3C and C1C) we observe the B-spline fit (i.e., a class of polynomial functions) to have the best predictive performance, compared to a linear fit (Fig. 3a). This indicates that a compositionally heterogeneous upwelling is most likely (Figs. 3a and 3c). However, minimal differences in predictive performance are observed between the single upwelling model (C1C 'heterogeneous' spline; RMSEP = 0.76) versus the small-scale upwelling model (C3C 'heterogeneous' spline; RMSEP = 0.75), assuming the distribution with distance is symmetrical across all rifts.

It is plausible that variable extension rates between the three rift systems [13] introduces further complexity to the geochemical and geophysical signals. Accordingly, we introduce three further models, C1D, C3D, and C3X (Figs. 2 and 3a; see Methods) to investigate how regional factors may influence upwelling behaviour. Models C1D and C3D consider one

upwelling and three small-scale upwellings, respectively, while allowing for distinct distance-dependent patterns for each rift, thereby modelling the distribution of each rift independently. Unlike the other models, C3X allows each small-scale upwelling to have a distinct signature, as well as permitting an independent distribution along each rift (Methods). We then obtain the optimum linear and B-spline fit for these three models. This analysis indicates that the overall best predictive model is the B-spline fit of C1D, wherein a single, heterogeneous mantle upwelling is present, albeit with differing distributions of key variables (Extended Data Table 2) between rift-arms. This model yields a mean standardised RMSEP of 0.59 (Fig. 3a). Whilst the Red Sea Rift and MER have a high sample density, the Gulf of Aden is lacking due to limited sample availability, however when excluding this the Gulf of Aden rift from our analyses the overall trend between the models remains the same (Extended Fig. 6). Using additional analysis, we confirm that excluding cases in which Ce/Pb < 20 does not affect our overall results (Extended Data Fig. 5), suggesting that primary mantle variations exert the first-order control on magma compositions. While the rifts share a common compositionally heterogenous upwelling, they appear to behave independently, which would imply that some feature of their tectonic regime modulates the observed signals.

Interplay Between Upwelling and Segmentation

We find that many of the optimum splines for each rift display distance-dependent sinusoidal patterns (Figs. 3c and Extended Data Fig. 2). Importantly, our analysis indicates that the variability observed for some indicators within the MER are of greater amplitude and shorter periodicity with distance compared to those of the Red Sea Rift (Fig. 3c and Extended Data Fig. 2). Further, the observed variation in Pb isotopes within the Red Sea Rift suggests that the upwelling may be chemically heterogeneous across some elements, but more uniform in others (i.e., $^{87}Sr/^{86}Sr$ and $^{143}Nd/^{144}Nd$). Although ΔNb values are broadly consistent across the region, we identify small-scale differences in La/Sm and Vs velocity at 100 km depth (within

171 the likely melt-rich zone in the asthenosphere [37]) with distance in each rift (Fig. 3c and
172 Extended Data Fig. 2). This feature likely indicates locally variable degrees of melting across
173 the region, which in turn raises the question: do the zones of locally higher melt fraction and
174 variable isotopic compositions observed in one rift correspond to those observed in the other
175 rifts?

176 To address this question, we carried out principal component analysis (PCA) and K-mean
177 cluster analysis using all variables post-standardisation. Across all variables, the K-means
178 cluster analysis algorithm seeks to group similar observations whilst minimising the within-
179 cluster total sum of squares for a pre-specified number of clusters. Our results from K-means
180 cluster analysis (Extended Data Fig. 4; Methods), show a higher number of clusters, smaller
181 in geographic size, assigned to the MER (50-100 km length scale, 4 repeating clusters)
182 compared to the Red Sea Rift (150-200 km length scale, 3 clusters). Several clusters are
183 found to co-exist in different rift-arms (clusters 1-3). For example, samples assigned to
184 cluster 3 are observed in the distal section of Red Sea Rift, as well as in locations closer to the
185 rift centre within the MER (Extended Data Fig. 4). The three clusters (1-3) observed across
186 the Red Sea Rift match the initial ~200 km clustering sequence observed across the MER.
187 This compositional similarity may indicate that they are derived from the same parent melt,
188 although the distribution of these melts within the MER appears to be more condensed over
189 shorter distances compared to the Red Sea Rift.

190 The spatial distribution of these clusters reflects variations in the composition and abundance
191 of melt (Extended Data Fig. 4) and shares some cursory similarities to the magmatic
192 segments (Extended Data Fig. 4). However, when inspected in detail we observe clear
193 differences. For example, volcanic systems both within magmatic segments and the adjacent
194 rift flanks are commonly allocated to single clusters, and the boundaries between clusters and
195 known magmatic segments are typically mismatched (Extended Data Fig. 4). In Afar, the

length scale of clusters is longer than that of magmatic segments. We therefore infer that the compositional variability is unlikely to be related to the along-axis segmentation of crustal subvolcanic plumbing systems.

Instead, we appeal to a deeper process. Taken together, our data can be explained through a pulsing upwelling model (e.g., [9]), as shown by the spline model and K-means cluster analysis. Rifts act as natural channels that are exploited by upwelling melt from deeper mantle sources [38]. Considering the extension rate in Afar (10.5-19.5 mm/yr; [19]) compared to that of the MER (~ 5.2 mm/yr; [19]), it is plausible that a mantle flow rate is impeded by the narrowing of the rift between Afar and the MER. This process would lead to a bottleneck effect [38, 39, 40], like that associated with the Galapagos plume [41]. This may in turn result in a different length-scale of mantle heterogeneity (Fig. 3; Extended Data Fig. 2) between the rifts (Extended Data Fig. 4). Further, a contrast in crustal thickness is evident between the rifts, with the MER crust being thicker (25-33 km) compared to that of Afar (16-25 km; Extended Data Fig. 1). This effect would likely introduce a difference in mantle flow rate. A progressive thickening of the overlying lithosphere away from the upwelling centre in the MER should reduce the volume capacity for melt, impeding the mantle flow. Consequently, the heterogeneous nature of the pulsating upwelling would likely exhibit a more condensed pattern within the MER compared to Afar, as we observe (Extended Data Fig. 4).

We conclude that variations in melt composition and abundance within Afar is best explained by a heterogeneous pulsing mantle upwelling that is not symmetrical (Extended Data Fig. 4), but instead shaped by varying extension rates within each rift (Fig. 4). Whilst this model principally investigates the likelihood of a singular or three-small-scale upwelling scenario, our results demonstrate that for either option, a heterogeneous upwelling provides the best match to observations in the region. The observed variations in melt composition and

abundance between the MER and Afar imply that the length scale of heterogeneities within magma-assisted rifting environments may be controlled not only by the upwelling itself but by the rift extension rate and crustal thickness. If this model is correct, it carries important implications for understanding the dynamical evolution of magmatism within continental rifts.

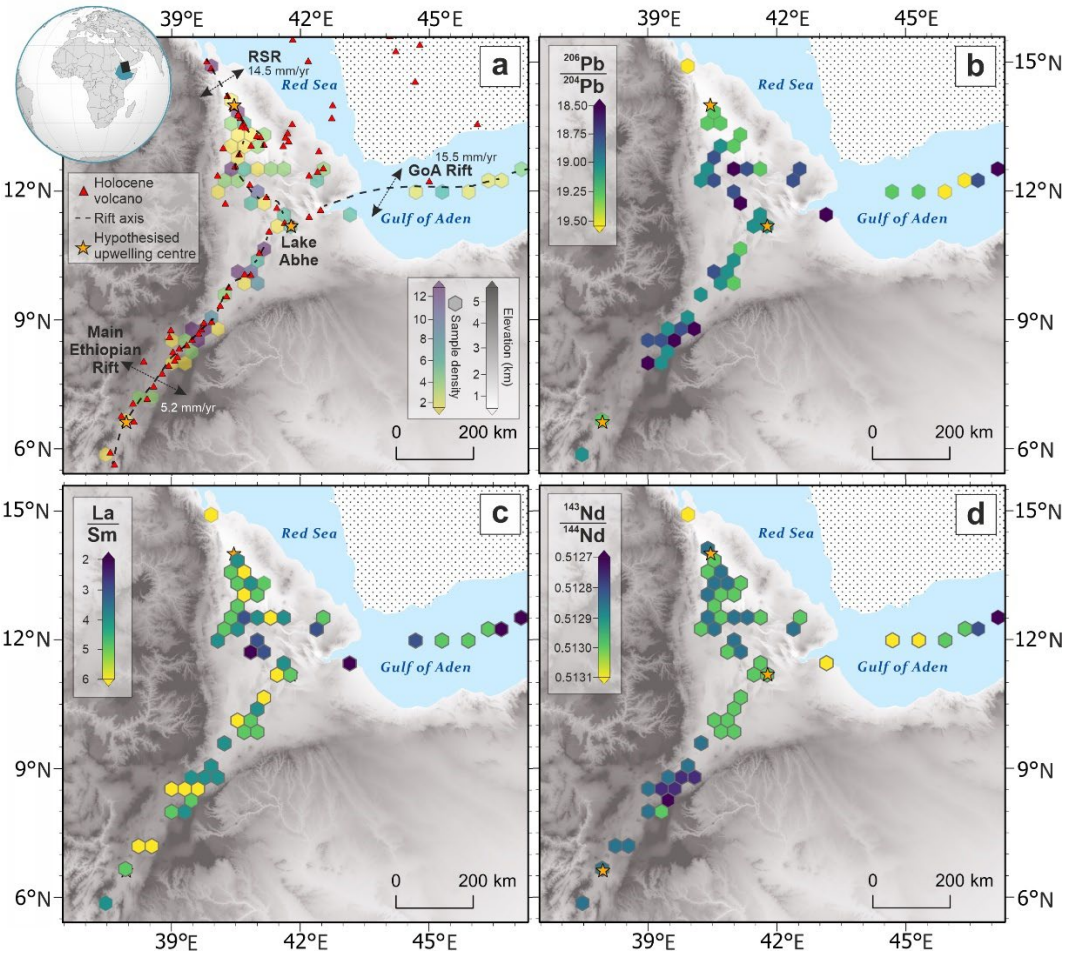

Fig. 1: Variation in geochemical and geophysical properties in the Afar triangle; (a) Map showing the Gulf of Aden (GoA) Rift, Red Sea Rift (RSR) and the Main Ethiopian Rift (MER) shown by a dashed line and associated rifting rates (after [19] & [20]). The three hypothesised [16, 30, 36] upwelling locations (yellow stars), Holocene volcanoes (red triangles) are shown. Hexplot colours show the density of samples within the hexagons' area with purple representing >12 and yellow showing 1-2. Location of maps shown on global inset (black rectangle) (b) Hexmap showing the $^{206}Pb/^{204}Pb$ variations across the study region (dark blue = low upwelling signature $^{206}Pb/^{204}Pb$, yellow = high $^{206}Pb/^{204}Pb$). (c) Hexmap showing the La/Sm variations across the study region (yellow = high La/Sm – high melt fraction, dark blue = low La/Sm – low melt fraction). (d) Hexmap showing the $^{143}Nd/^{144}Nd$ variations across the study region. Yellow indicates a high upwelling-like $^{143}Nd/^{144}Nd$, dark blue = low $^{143}Nd/^{144}Nd$).

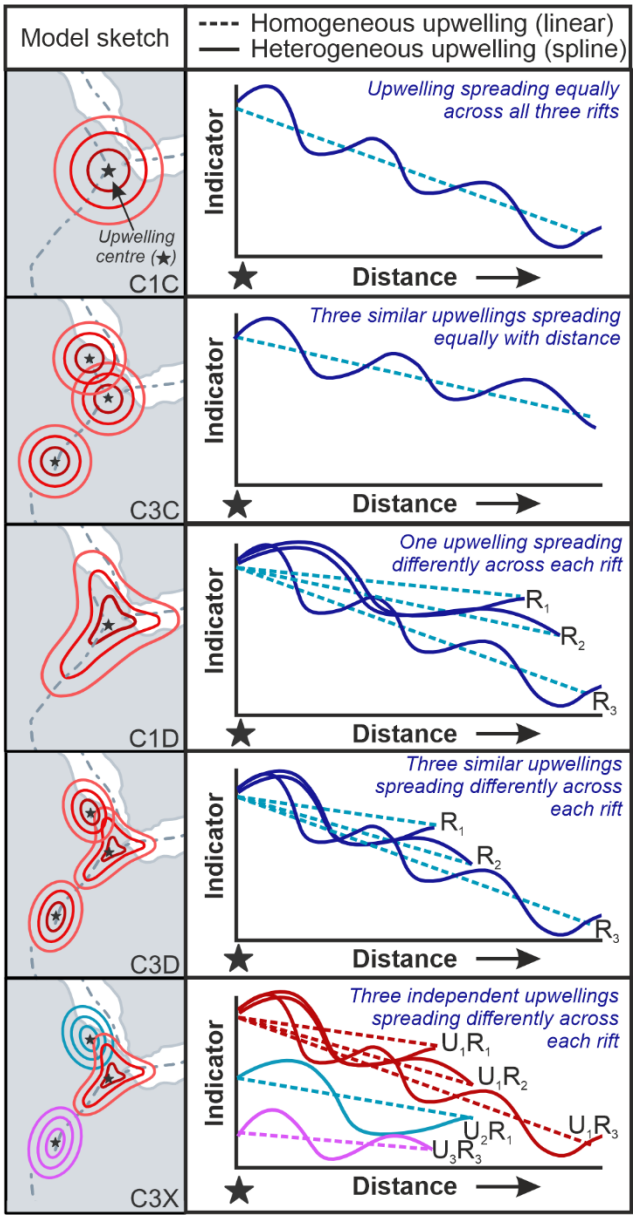

239

240 **Fig. 2: Models of mantle upwellings beneath Afar tested in this study;** Schematic diagram
241 of the upwelling scenarios for Afar that were tested within this study. The diagrams (left) are
242 labelled with the code associated with each model (see Table A1 and the Statistical Analyses
243 section within Methods for further details). The number of lines, shown on the schematic
244 graphs (right), equals the number of models that must be fitted for that model variant (linear
245 = dashed, spline = continuous). Note that each model variant has been illustrated with an
246 indicator that decreases with a reduction in upwelling proportion. The location of the mantle
247 upwelling(s) is shown by the star symbol.

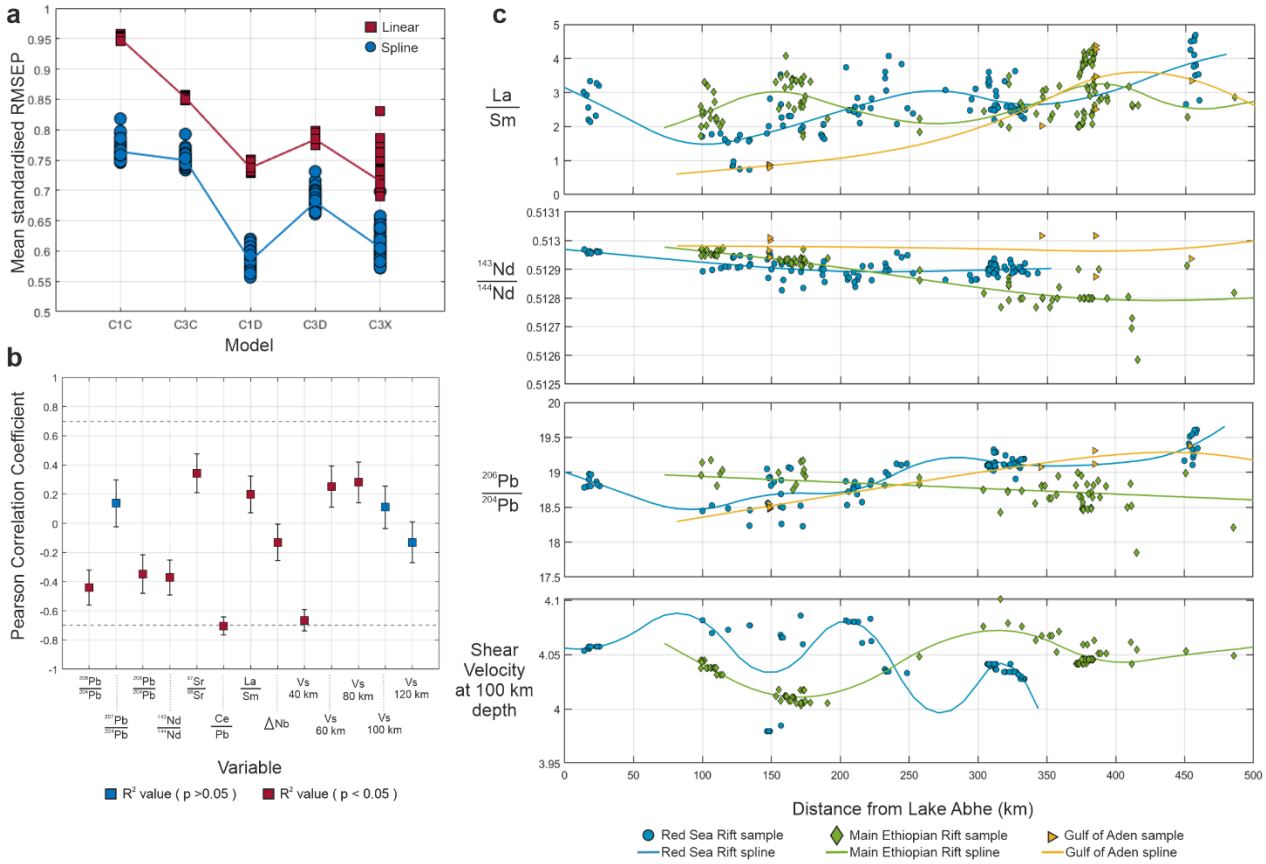

Fig. 3: Statistical analysis of Afar rift properties; (**a**) The mean standardised root means square error of prediction (RMSEP) for each of the models tested. Individual linear model results are shown by red squares and the mean of those results are displayed by the red line. Individual spline results are shown by blue circles and the mean of those results are shown by a blue line. (**b**) Pearson correlation coefficient of each of the selected 13 variables with Moho depth. Error bars show the 95-percentile error of the coefficient. Red squares indicate where the correlation is significant ($p < 0.05$) and blue squares indicate that the correlations are not deemed significant ($p > 0.05$). (c) Splines (lines) of the winning model (C1C) for selected variables. Symbols show the data within the study (blue circles = Red Sea Rift, green diamonds = Main Ethiopian Rift, yellow triangles = Gulf of Aden Rift).

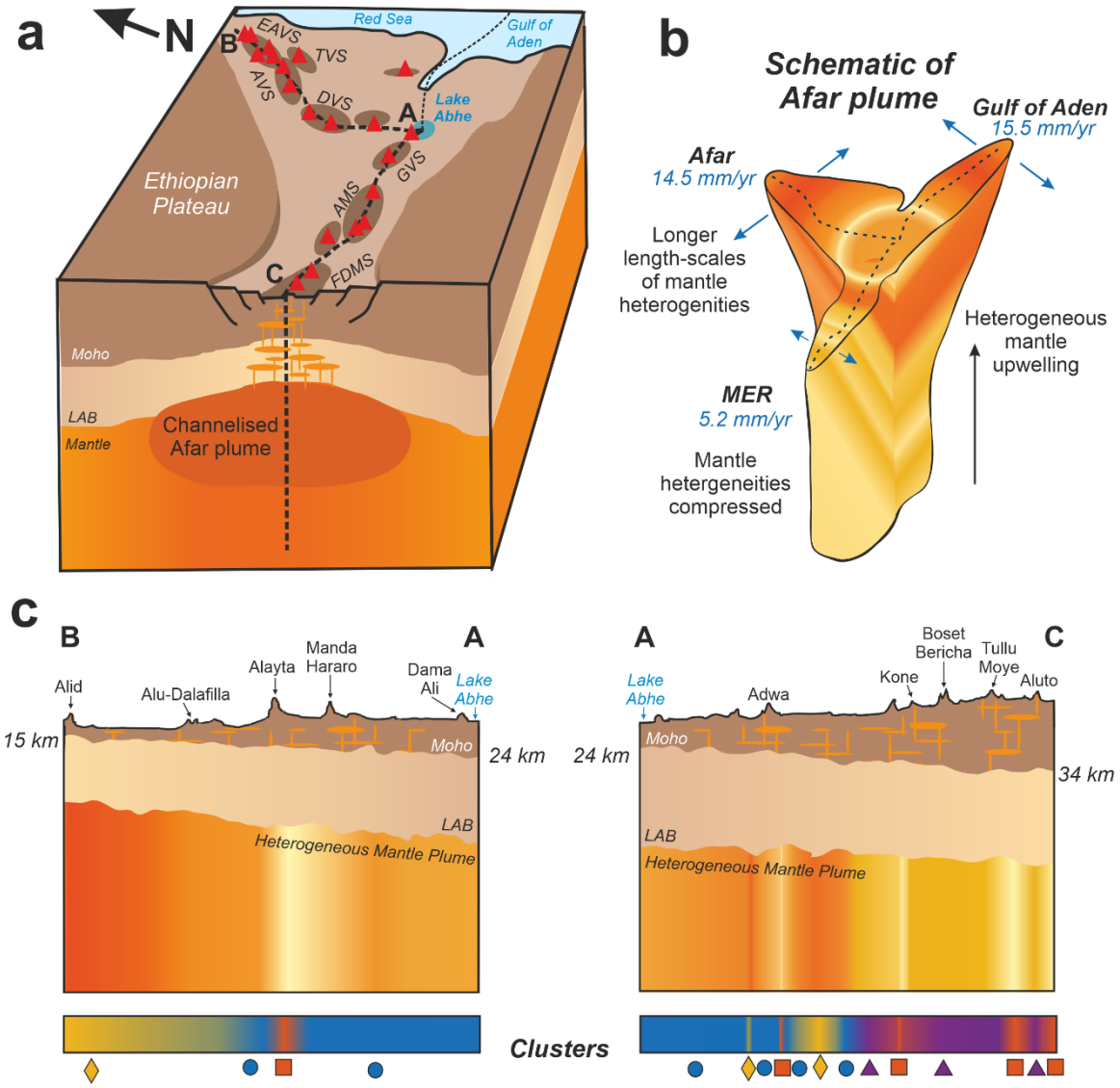

Fig. 4: Spatially heterogeneous nature of the mantle upwelling beneath Afar. (**a**) Box diagram showing the rifts across Afar and the mantle upwelling being channelised by the rift. The lines of section A-B-C are those drawn in (c). (**b**) Schematic of the Afar upwelling showing the dimensions of channelised flow along the three rifts (dashed lines). (**c**) Schematic cross sections along the Red Sea Rift (A-B) and MER (A-C) showing the distribution of heterogeneities within the mantle upwelling and how that links to the clusters shown in Extended Data Fig. A4.

References

[1] Cañón-Tapia, E., Walker, G.P.L.: Global aspects of volcanism: the perspectives of "plate tectonics" and "volcanic systems". Earth-Science Reviews 66(1-2), 163–182 (2004) https://doi.org/10.1016/j.earscirev.2003.11.001

[2] Morgan, W.J.: Convection Plumes in the Lower Mantle. Nature 1971 230:5288 230 (5288), 42–43 (1971) https://doi.org/10.1038/230042a0

[3] White, R., McKenzie, D.: Magmatism at rift zones: the generation of volcanic continental margins and flood basalts. Journal of Geophysical Research 94(B6), 7685–7729 (1989) https://doi.org/10.1029/JB094IB06P07685

[4] Rooney, T.O.: The Cenozoic magmatism of East Africa: Part IV – The terminal stages of rifting preserved in the Northern East African Rift System. Lithos 360-361 (2020) https://doi.org/10.1016/j.lithos.2020.105381

[5] Schilling, J.-G.: Afar Mantle Plume: Rare Earth Evidence. Nature Physical Science 242(114), 2–5 (1973) https://doi.org/10.1038/physci242002a0

[6] Rychert, C.A., Hammond, J.O.S., Harmon, N., Michael Kendall, J., Keir, D., Ebinger, C., Bastow, I.D., Ayele, A., Belachew, M., Stuart, G.: Volcanism in the Afar Rift sustained by decompression melting with minimal plume influence. Nature Geoscience 5(6), 406–409 (2012) https://doi.org/10.1038/ngeo1455

[7] Ito, G.: Reykjanes 'V'-shaped ridges originating from a pulsing and dehydrating mantle plume. Nature 2001 411:6838 411(6838), 681–684 (2001) https://doi.org/10.1038/35079561

[8] Parkin, C.J., Lunnon, Z.C., White, R.S., Christie, P.A.F.: Imaging the pulsing Iceland mantle plume through the Eocene. Geology 35(1), 93 (2007) https://doi.org/10.1130/G23273A.1

290 [9] Taylor, R.N., Davila-Harris, P., Branney, M.J., Ruth Farley, E.M., Gernon, T.M., Palmer,
291 M.R.: Dynamics of a chemically pulsing mantle plume. Earth and Planetary Science Letters
292 537, 116182 (2020) https://doi.org/10.1016/j.epsl.2020.116182

293 [10] Weis, D., Harpp, K.S., Harrison, L.N., Boyet, M., Chauvel, C., Farnetani, C.G.,
294 Finlayson, V.A., Lee, K.K.M., Parai, R., Shahar, A., Williamson, N.M.B. Earth's mantle
295 composition revealed by mantle plumes. Nature Reviews Earth & Environment 4(9), 604–
296 625 (2023) https://doi.org/10.1038/s43017-023-00467-0

297 [11] Jackson, M.G., Becker, T.W., Steinberger, B.: Spatial Characteristics of Recycled and
298 Primordial Reservoirs in the Deep Mantle. Geochemistry, Geophysics, Geosystems 22(3)
299 (2021) https://doi.org/10.1029/2020GC009525

300 [12] Rogers, N., Macdonald, R., Fitton, J.G., George, R., Smith, M., Barreiro, B.: Two mantle
301 plumes beneath the East African rift system: Sr, Nd and Pb isotope evidence from Kenya Rift
302 basalts. Earth and Planetary Science Letters (2000) https://doi.org/10.1016/S0012-
303 821X(00)00012-1

304 [13] Zwaan, F., Corti, G., Keir, D., Sani, F.: A review of tectonic models for the rifted margin
305 of Afar: Implications for continental break-up and passive margin formation. Journal of
306 African Earth Sciences 164, 103649 (2020) https://doi.org/10.1016/j.jafrearsci.2019.103649

307 [14] Ferguson, D.J., MacLennan, J., Bastow, I.D., Pyle, D.M., Jones, S.M., Keir, D., Blundy,
308 J.D., Plank, T., Yirgu, G.: Melting during late-stage rifting in Afar is hot and deep. Nature
309 499(7456), 70–73 (2013) https://doi.org/10.1038/nature12292

310 [15] Hansen, S.E., Nyblade, A.A.: The deep seismic structure of the Ethiopia/Afar hotspot
311 and the African superplume. Geophysical Journal International 194(1), 118–124 (2013)
312 https://doi.org/10.1093/gji/ggt116

313 [16] Schilling, J.G., Kingsley, R.H., Hanan, B.B., McCully, B.L.: Nd-Sr-Pb isotopic
314 variations along the Gulf of Aden: evidence for Afar mantle plume-continental lithosphere
315 interaction. Journal of Geophysical Research 97(B7) (1992)
316 https://doi.org/10.1029/92jb00415

317 [17] Hagos, M., Koeberl, C., Vries, B.: The Quaternary volcanic rocks of the northern Afar
318 Depression (northern Ethiopia): Perspectives on petrology, geochemistry, and tectonics.
319 Journal of African Earth Sciences 117, 29–47 (2016)
320 https://doi.org/10.1016/J.JAFREARSCI.2015.11.022

321 [18] Smithsonian Institution: Global Volcanism Program (2013)

322 [19] Zwaan, F., Corti, G., Sani, F., Keir, D., Muluneh, A.A., Illsley-Kemp, F., Papini, M.:
323 Structural Analysis of the Western Afar Margin, East Africa: Evidence for Multiphase
324 Rotational Rifting. Tectonics 39(7) (2020) https://doi.org/10.1029/2019TC006043

325 [20] Gillard, M., Leroy, S., Cannat, M., Sloan, H.: Margin-to-Margin Seafloor Spreading in
326 the Eastern Gulf of Aden: A 16 Ma-Long History of Deformation and Magmatism from
327 Seismic Reflection, Gravity and Magnetic Data. Frontiers in Earth Science 9 (2021)
328 https://doi.org/10.3389/feart.2021.707721

329 [21] DIGIS Team: GEOROC Compilation: Rift Volcanics (2021).
330 https://doi.org/10.25625/KAIVCT

331 [22] Chambers, E.L., Harmon, N., Rychert, C.A., Gallacher, R.J., Keir, D.: Imaging the
332 seismic velocity structure of the crust and upper mantle in the northern East African Rift
333 using Rayleigh wave tomography. Geophysical Journal International 230(3), 2036–2055
334 (2022) https://doi.org/10.1093/gji/ggac156

335 [23] Hanan, B.B., Graham, D.W.: Lead and Helium Isotope Evidence from Oceanic Basalts
336 for a Common Deep Source of Mantle Plumes. Science 272(5264), 991–995 (1996)
337 https://doi.org/10.1126/science.272.5264.991

338 [24] Benoit, M.H., Nyblade, A.A., VanDecar, J.C.: Upper mantle P-wave speed variations
339 beneath Ethiopia and the origin of the Afar hotspot. Geology 34(5), 329–332 (2006)
340 https://doi.org/10.1130/G22281.1

341 [25] Ritsema, J., Allen, R.M.: The elusive mantle plume. Earth and Planetary Science Letters
342 207(1-4), 1–12 (2003) https://doi.org/10.1016/S0012-821X(02)01093-2

343 [26] Hart, S.R., Hauri, E.H., Oschmann, L.A., Whitehead, J.A.: Mantle Plumes and
344 Entrainment: Isotopic Evidence. Science 256(5056), 517–520 (1992)
345 https://doi.org/10.1126/SCIENCE.256.5056.517

346 [27] Fitton, J.G., Saunders, A.D., Norry, M.J., Hardarson, B.S., Taylor, R.N.: Thermal and
347 chemical structure of the Iceland plume. Earth and Planetary Science Letters 153(3-4), 197–
348 208 (1997) https://doi.org/10.1016/S0012-821X(97)00170-2

349 [28] Pik, R., Marty, B., Hilton, D.R.: How many mantle plumes in Africa? The geochemical
350 point of view. Chemical Geology 226(3-4), 100–114 (2006)
351 https://doi.org/10.1016/j.chemgeo.2005.09.016

352 [29] Chambers, E.L., Harmon, N., Keir, D., Rychert, C.A.: Using Ambient Noise to Image
353 the Northern East African Rift. Geochemistry, Geophysics, Geosystems 20(4), 2091–2109
354 (2019) https://doi.org/10.1029/2018GC008129

355 [30] Civiero, C., Armitage, J.J., Goes, S., Hammond, J.O.S.: The Seismic Signature of
356 Upper-Mantle Plumes: Application to the Northern East African Rift. Geochemistry,
357 Geophysics, Geosystems 20(12), 6106–6122 (2019) https://doi.org/10.1029/2019GC008636

358 [31] Gallacher, R.J., Keir, D., Harmon, N., Stuart, G., Leroy, S., Hammond, J.O.S., Kendall,
359 J.-M., Ayele, A., Goitom, B., Ogubazghi, G., Ahmed, A.: The initiation of segmented
360 buoyancy-driven melting during continental breakup. Nature Communications 7(1), 13110
361 (2016) https://doi.org/10.1038/ncomms13110

362 [32] Abouchami, W., Hofmann, A.W., Galer, S.J.G., Frey, F.A., Eisele, J., Felgenson, M.:
363 Lead isotopes reveal bilateral asymmetry and vertical continuity in the Hawaiian mantle
364 plume. Nature 434(7035), 851–856 (2005) https://doi.org/10.1038/nature03402

365 [33] Hutchison, W., Mather, T.A., Pyle, D.M., Boyce, A.J., Gleeson, M.L.M., Yirgu, G.,
366 Blundy, J.D., Ferguson, D.J., Vye-Brown, C., Millar, I.L., Sims, K.W.W., Finch, A.A.: The
367 evolution of magma during continental rifting: New constraints from the isotopic and trace
368 element signatures of silicic magmas from Ethiopian volcanoes. Earth and Planetary Science
369 Letters 489, 203–218 (2018) https://doi.org/10.1016/j.epsl.2018.02.027

370 [34] Illsley-Kemp, F., Keir, D., Bull, J.M., Gernon, T.M., Ebinger, C., Ayele, A., Hammond,
371 J.O.S., Kendall, J.M., Goitom, B., Belachew, M.: Seismicity During Continental Breakup in
372 the Red Sea Rift of Northern Afar. Journal of Geophysical Research: Solid Earth 123(3),
373 2345–2362 (2018) https://doi.org/10.1002/2017JB014902

374 [35] Hofmann, A.W., Jochum, K.P., Seufert, M., White, W.M.: Nb and Pb in oceanic basalts:
375 new constraints on mantle evolution. Earth and Planetary Science Letters 79(1-2), 33–45
376 (1986) https://doi.org/10.1016/0012-821X(86)90038-5

377 [36] Rooney, T.O., Hanan, B.B., Graham, D.W., Furman, T., Blichert-Toft, J., Schilling, J.-
378 G.: Upper Mantle Pollution during Afar Plume–Continental Rift Interaction. Journal of
379 Petrology 53(2), 365–389 (2012) https://doi.org/10.1093/petrology/egr065

380 [37] Armitage, J.J., Ferguson, D.J., Goes, S., Hammond, J.O.S., Calais, E., Rychert, C.A.,
381 Harmon, N.: Upper mantle temperature and the onset of extension and break-up in Afar,

382 Africa. Earth and Planetary Science Letters 418, 78–90 (2015)
383 https://doi.org/10.1016/j.epsl.2015.02.039

384 [38] Ebinger, C.J., Sleep, N.H.: Cenozoic magmatism throughout east Africa resulting from
385 impact of a single plume. Nature 395, 788–791 (1998) https://doi.org/10.1038/27417

386 [39] Chang, S.J., Lee, S.: Mantle plumes and associated flow beneath Arabia and East Africa.
387 Earth and Planetary Science Letters 302(3-4), 448–454 (2011)
388 https://doi.org/10.1016/j.epsl.2010.12.050

389 [40] Hansen, Anders Hedegaard. "Flow Through Restriction." In Fluid Power Systems: A
390 Lecture Note in Modelling, Analysis and Control, pp. 43-61. Cham: Springer International
391 Publishing, (2023). https://doi.org/10.1007/978-3-031-15089-0_4

392 [41] Naif, Samer, Nathaniel C. Miller, Donna J. Shillington, Anne Bécel, Daniel Lizarralde,
393 Dan Bassett, and Sidney R. Hemming. "Episodic intraplate magmatism fed by a long-lived
394 melt channel of distal plume origin." Science Advances 9, no. 23 (2023): eadd3761
395 https://doi.org/10.1126/sciadv.add3761